Electrochemical Investigation of a CT Complex and its Applications in Energy Storage Systems

I. S. El-Hallag[1*], A. A. Al-Owais[2] and E. H. El-Mossalamy[3]

[1]*Chemistry Department, Faculty of Science, Tanta University, Tanta, Egypt*
[2]*Chemistry Department, College of Science, King Saud University, Riyadh, Saudi Arabia*
[3]*Chemistry Department, Faculty of Science, Benha University, Benha, Egypt*
*Corresponding author: i.elhallag@yahoo.com

Received 11/11/2025; accepted 20/05/2026
https://doi.org/10.4152/pea.2027450602

Abstract

Charge-transfer (CT) complex exhibits unique redox properties that make it a promising candidate for advanced energy storage and conversion systems. This study presents a comprehensive electrochemical investigation of CT complex, focusing on its charge-storage behavior and kinetic characteristics. Quantitative analysis revealed high specific capacitance (C_{sp}) values derived from cyclic voltammetry (CV) and galvanostatic charge–discharge (GCD) measurements, ranging from 494 to 114 F/g (CV) and 490 to 117 F/g (GCD) over scan rate range from 0.025 to 0.40 V/s. This demonstrates good rate capability and strong agreement between both electrochemical methods. Tafel analysis further provided insights into onset potential and exchange current density, confirming efficient electron transfer. This novel approach converts CV data into galvanostatic charge-discharge profiles, enabling accurate C_{sp} evaluation of CT complex from a single electrochemical dataset. Integration of CV-derived GCD and Tafel plots provides a good methodological framework for correlating pseudocapacitive behavior with CT kinetics. These findings highlight the potential of CT complex as an efficient, low-cost and tunable material for supercapacitors and electrocatalytic energy storage devices.

***Keywords*:** Charge-transfer complex; Pseudocapacitance; Tafel plot.

Introduction•

Charge-transfer (CT) complex is a molecular system formed through interactions between electron-rich donor molecules and electron-deficient acceptors [1, 2]. This complex exhibits unique optical, magnetic and electronic characteristics, making it a promising candidate for molecular electronics, catalysis, sensors and energy storage devices [3-6]. Recently, investigation of CT complex using electrochemical techniques has gained momentum, due to the need for detailed mechanistic insights into electron transfer reactions [7, 8]. Among the suite of electrochemical methods, cyclic voltammetry (CV) remains a powerful diagnostic tool to probe redox processes, reversibility and electrode kinetics [9-12]. The use

•The abbreviations list is in page 703.

of electrochemical techniques to characterize CT complex not only advances the understanding of its redox chemistry but also facilitates the design of materials with enhanced performance for electrochemical capacitors and sensors [13, 14]. Notably, the integration of CV plot data allows for comprehensive evaluation of specific capacitance (C_{sp}) [15]. The transformation of a CV to a galvanostatic charge–discharge GCD plot is particularly valuable for exploratory studies, where rapid screening of electrode materials is required and traditional GCD experiments may be impractical [16]. CV-to-GCD conversion method offers significant practical advantages, as it enables the extraction of charge–discharge characteristics and C_{sp} directly from CV data without the need for separate galvanostatic measurements. This approach is especially beneficial for rapid material screening, limited sample quantities and preliminary performance evaluation in laboratory-scale studies. By utilizing a single electrochemical dataset, the method improves experimental efficiency, reduces time consumption and allows direct correlation between redox behavior and charge-storage capability. Its application is particularly suitable for predominantly capacitive and pseudocapacitive systems, where surface-controlled processes dominate electrochemical response. However, derived C_{sp} values represent an upper bound, as CV currents are not constant during charging/discharging and may include contributions from non-capacitive processes, e.g., diffusion-controlled reactions [17]. The method is therefore best used in conjunction with true galvanostatic cycling to confirm quantitative metrics [18]. Recent studies further underscore rapid developments in electrochemical energy storage and characterization of pseudocapacitive systems. For example, a comprehensive review on CV characterization of hybrid supercapacitors highlights latest methodologies that link voltammetric analysis with device performance, reinforcing the relevance of integrating CV-derived metrics with charge-discharge evaluation [16, 19]. In addition, reviews on advanced pseudocapacitive materials emphasize the importance of redox-active systems with tunable physicochemical properties and rapid kinetics for high-performance supercapacitor applications [20]. Studies on metal–organic framework-based composite electrodes and hybrid device architectures published in 2025 also demonstrate how innovative material designs can enhance specific capacitance and cycling stability, situating the present work within current trends in electrode development and electrochemical analysis [21, 22]. In the present study, CT complex involving 4,4'-bipyridine and substituted benzoquinone derivatives was synthesized and characterized. CV technique was herein employed to explore the complex's electrochemical behavior under various scan rates [23-25]. In addition to its unique redox activity, CT complex is increasingly explored for its potential in energy storage applications. The intrinsic donor-acceptor interactions within CT systems facilitate efficient electron transfer, enabling it to function as a pseudocapacitive material with promising charge storage capability [9, 13]. Its reversible redox transitions contribute to rapid charge-discharge processes, while tunable

molecular structures allow optimization of its electrochemical performance. Moreover, CT complex often exhibits remarkable long-term electrochemical stability, maintaining capacitance retention over extended cycling, which is a critical requirement for practical supercapacitor and battery applications. These properties make CT complex an attractive candidate for next-generation energy storage devices, bridging the gap between molecular design and electrochemical functionality.

Experimental and methods

Materials

All reagents were of analytical grade and used as-received, unless otherwise noted. Solvents were purified and dried according to standard procedures. 2,3-Dichloro-5,6-dicyano-1,4-benzoquinone (DDQ) and 4,4′-bipyridine (BPy) were purchased from Aldrich Chemical Co. and employed without further purification.

Synthesis of solid charge transfer complex

Equimolar solutions (5 mM) of BPy and each DDQ derivative were prepared in methanol. CT complexes were synthesized by mixing equal volumes (1:1 v/v) of donor (BPy) and acceptor (DDQ) solutions under stirring, at room temperature, for 30 min. The resulting colored solution was stored in an amber bottle and used directly for electrochemical studies. No additional purification was carried out; the synthesis process yields BPy-DDQ CT complex (Fig. 1).

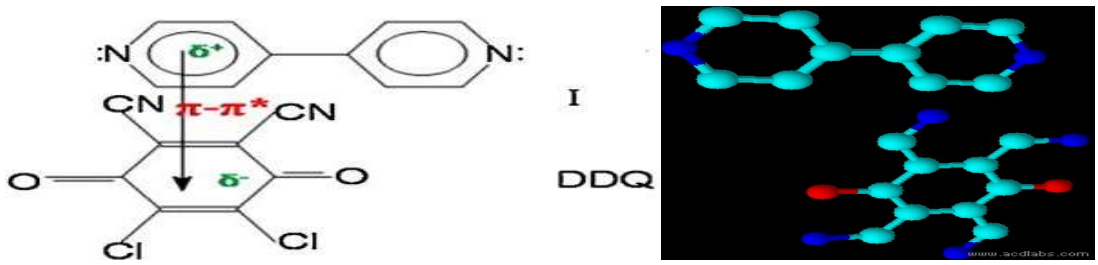

Figure 1: BPy-DDQ CT complex's skeletal structure.

Electrochemical measurements

Electrochemical experiments were carried out using an EG&G Potentiostat Model 283 electrochemical workstation. A conventional three-electrode cell was employed, consisting of gold working electrode, platinum wire counter electrode, and Ag/AgCl reference electrode (saturated or 3.0 M KCl, as specified). Measurements were conducted at 23 ± 2 °C in anhydrous dichloromethane containing 0.1 M tetra-ethylammonium perchlorate (TEAP). CV was performed within a potential range from –0.2 to + 0.8 V vs. Ag/AgCl at scan rates ranging from 0.025 to 0.4 V/s. Prior to

all measurements, the solutions were purged with oxygen-free nitrogen for ≥15 min, and a nitrogen blanket was maintained throughout.

Results and discussion

Cyclic voltammetry characterization

CV of BPy-DDQ CT-complex exhibits scan-rate dependent, quasi-reversible redox behavior indicative of diffusion-limited processes [7, 8]. It was noted that, as scan rate increased (from 0.025 to 0.4 V/s), peak currents grew and anodic-cathodic peak separation increased (Fig. 2), indicating finite heterogeneous electron-transfer kinetics and uncompensated resistive or ohmic effects [11]. CV shape also includes a broad, sloping background current that reflects capacitive (double-layer and pseudocapacitive) contributions arising from the high surface area hierarchical morphology of the complex [13, 14, 18]. Together, these observations imply a redox mechanism in which primary faradaic processes are facilitated by intimate π–π stacked donor–acceptor domains at the electrode interface, while long-range ionic transport into and out of aggregated domains imposes a diffusion limitation at higher rates [1, 2, 24].

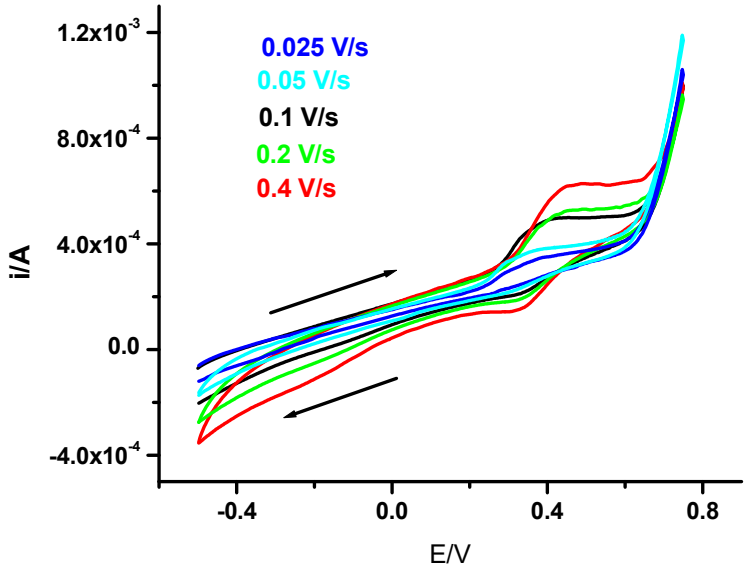

Figure 2: CV of BPy–DDQ CT complex at a Au electrode in 0.1 M TEAP/CH_2Cl_2, recorded at scan rates from 0.025 to 0.4 V/s.

From CV to GCD

A novel route to evaluate capacitance in CT complex

In this work, a methodology for converting CV data into GCD profiles is introduced, enabling the evaluation of specific capacitance directly from CV experiments. Unlike traditional approaches where CV and GCD are treated as independent techniques, this method bridges both by numerically transforming current-potential data into potential-time behavior. This framework not only reduces experimental redundancy, but also provides new insight into

pseudocapacitive contributions of CT complex, where faradaic and capacitive processes often coexist. By validating converted profiles against experimental GCD curves, it is herein demonstrated that this approach represents a promising diagnostic and comparative tool for supercapacitor research and a novel pathway for extracting electrochemical parameters from a single dataset. Fig. 3 indicates the novel CV–GCD conversion method for capacitance evaluation of CT complex.

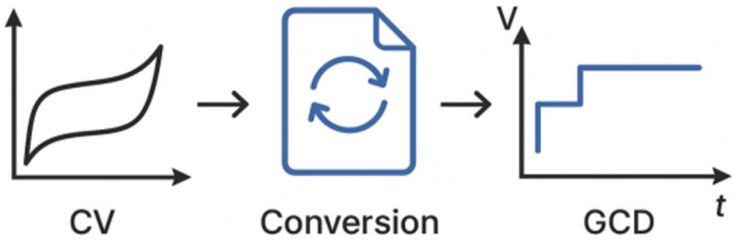

Figure 3: CV-to-GCD conversion for capacitance evaluation of CT complex.

Electrochemical characterization of CT complex commonly utilizes CV as main diagnostic technique [9]. Although CV curves provide valuable qualitative and semi-quantitative insights [25], precise determination of gravimetric specific capacitance (C_{sp}) is more reliably achieved using GCD measurements, where potential–time response is monitored under a constant current condition [10]. In cases where GCD measurements are unavailable, or where CV data are more readily acquired, it is possible to computationally reconstruct a GCD-like profile from CV datasets. This allows quantitative extraction of C_{sp} from potential-time behavior derived from potential-current relationships [15, 16]. Fig. 4 presents charging-discharging of *E-t* plot at various scan rates.

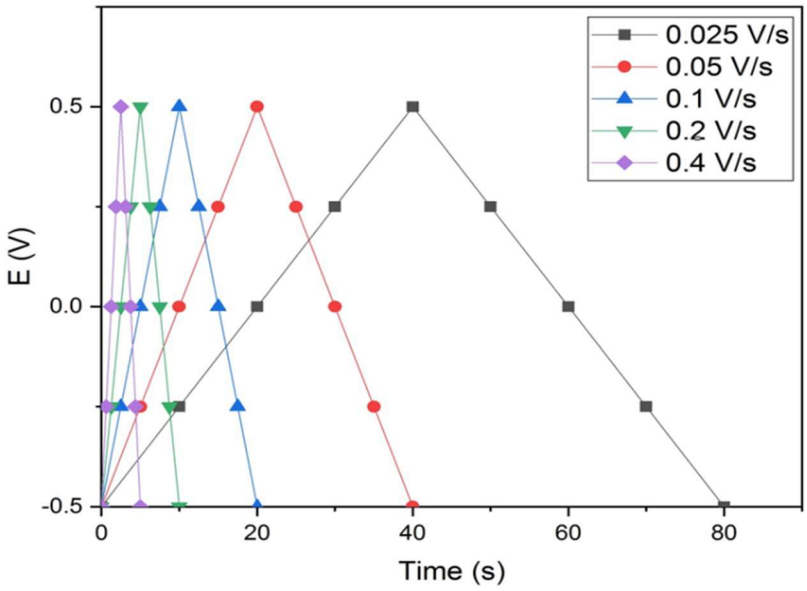

Figure 4: Triangular *E–t* (GCD-like) plot generated by converting CV data recorded at a Au electrode in 0.1 M TEAP/CH_2Cl_2 at scan rates of 0.025–0.4 V/s.

E–t plots reveal that the CT complex exhibits stable, reversible pseudocapacitive behavior with efficient charge-discharge characteristics. The performance is highly scan-rate dependent, as low scan rates favor higher capacitance due to better ion access, while high scan rates favor rapid charge-discharge cycles suitable for high-power applications.

Principle of conversion from CV to GCD

In the CV, the working electrode potential (*E*) is swept linearly with time at a constant scan rate (*v*, in V/s), while current (*i*) is recorded [26, 27]. The fundamental relationship governing CV is indicated in Eq. (1):

$$dE/dt = v \quad (1)$$

where *E* is the electrode potential in volts (V), t the time in sec, *dE*/*dt* is the rate of change of potential with time, known as scan rate, and ν is , potential scan rate in volts per second (V/s).

Thus, time corresponding to each potential point can be obtained via Eq. (2):

$$t = (E\text{-}E_{start})/v \quad (2)$$

where E_{start} is initial potential of the sweep. For a full CV cycle, both forward (anodic) and reverse (cathodic) scans can be mapped onto a continuous time axis by sequentially applying the above relation with the appropriate sign for Δ*E* [28-30]. To perform a GCD curve, forward CV sweep (charging) was interpreted as charge segment and reverse sweep (discharging) as discharge segment. While a real GCD experiment maintains constant current, CV-based approach uses measured instantaneous current at each potential to approximate average current (I_{av}) which is average constant current for charging and discharging steps. This average constant current is inserted into GCD capacitance equation [31-34].

Experimental data transformation

For the CT complex under investigation (BPy-DDQ), CV data were acquired at an Au disc electrode loaded by the mass of the CT-complex in 0.1 M TEAP in dichloromethane at various scan rates. Potential range was from -0.2 to +0.8 V, followed by a reverse sweep back to -0.2 V. Recorded currents (*i*) in amperes were paired with potentials to create an ordered dataset. Time (Δt) corresponding to each potential increment (Δ*E*) was calculated using Eq. (3).

$$\Delta t = |\Delta E|/v \quad (3)$$

This yielded a complete potential-time table, analogous to a GCD dataset, with time progressing over full charge-discharge cycle [35-37].

Specific capacitance calculation

Specific capacitance (C_{sp}) was obtained from the discharge portion of reconstructed GCD curve, according to Eq. (4) [38-41]:

$$Csp = \frac{I_{av}.\Delta t}{m\Delta V} \quad (4)$$

where I_{av} is average constant current as defined before, Δt is discharge time, m is mass of active material and ΔV is potential drop during discharge.

From the CV, one can obtain average constant current (I_{av}) using the amount of charge (Q) via Eq. (5):

$$I_{\mathrm{av}} = \frac{Q}{\Delta t} \quad (5)$$

$$Q = \int_{t_{\mathrm{start}}}^{t_{\mathrm{end}}} I(t)\, dt \quad (6)$$

where Δt is obtained from $\Delta t = \frac{\Delta V}{v}$.

C_{sp} values of BPy-DDQ CT complex calculated from both CV and GCD [42-45] methods are summarized in Table 1.

Table 1: Values of *C*sp calculated via CV and GCD methods at various scan rates.

Scan rate (*v*)	Specific capacitance	
(V/s)	CV (F/g)	GCD (F/g)
0.025	494	490
0.050	360	356
0.100	303	300
0.200	231	234
0.400	114	117

A strong correlation between the two techniques was observed across the entire scan rates range. At 0.025 V/s, the capacitance obtained from CV (494 F/g) was nearly identical to that from GCD (490 F/g), while similar agreement was maintained at higher scan rates, e.g., 303 *vs*. 300 F/g at 0.1 V/s and 114 *vs*. 117 F/g at 0.4 V/s.

Close correspondence between CV- and GCD-derived capacitances confirms the reliability and reproducibility of electrochemical measurements. Moreover, gradual decrease in C_{sp} with increasing scan rate reflects limited accessibility of redox-active sites at higher sweep speeds, which is a typical feature of pseudocapacitive systems. These results underscore that both methods consistently capture charge-storage behavior of CT complex, validating its efficient and reversible redox activity.

Comparative bar graph (Fig. 5) illustrates C_{sp} values obtained from CV and GCD at different scan rates.

At all scan rates, capacitances determined by both methods are nearly identical, with only minor deviations of less than 2%. This strong agreement demonstrates the consistency and reliability of the electrochemical evaluation methods, confirming that charge-storage behavior of BPy-DDQ CT complex is accurately captured by both techniques.

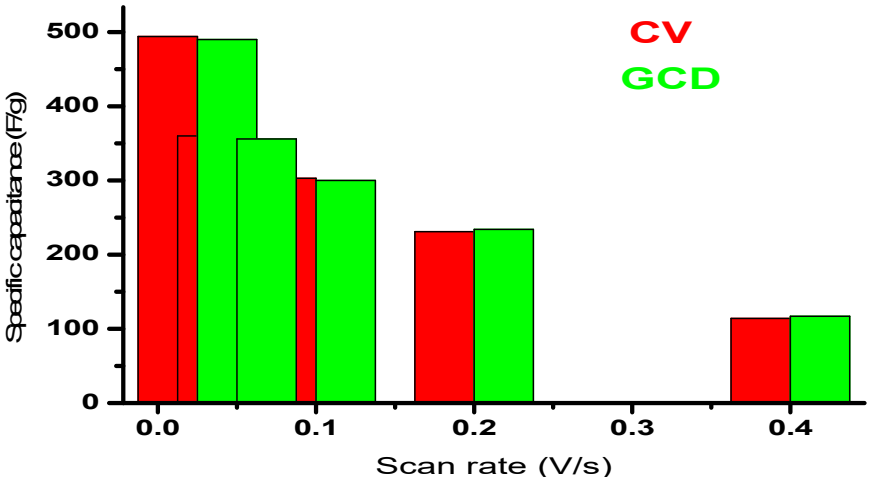

Figure 5: Correspondence between C_{sp} values obtained from CV and GCD at an Au electrode in 0.1 M TEAP/CH_2Cl_2, recorded at scan rates from 0.025 to 0.4 V/ s.

As shown in Fig. 6, scatter plot comparing CV- and GCD-derived capacitances reveals an excellent linear correlation, with all data points lying very close to ideal y = x line. Calculated coefficient of determination (R^2) was 0.9993, confirming near-perfect agreement between both electrochemical methods. This strong correlation quantitatively validates the reliability of capacitance values, demonstrating that both CV and GCD provide consistent assessments of charge-storage behavior of BPy-DDQ CT complex.

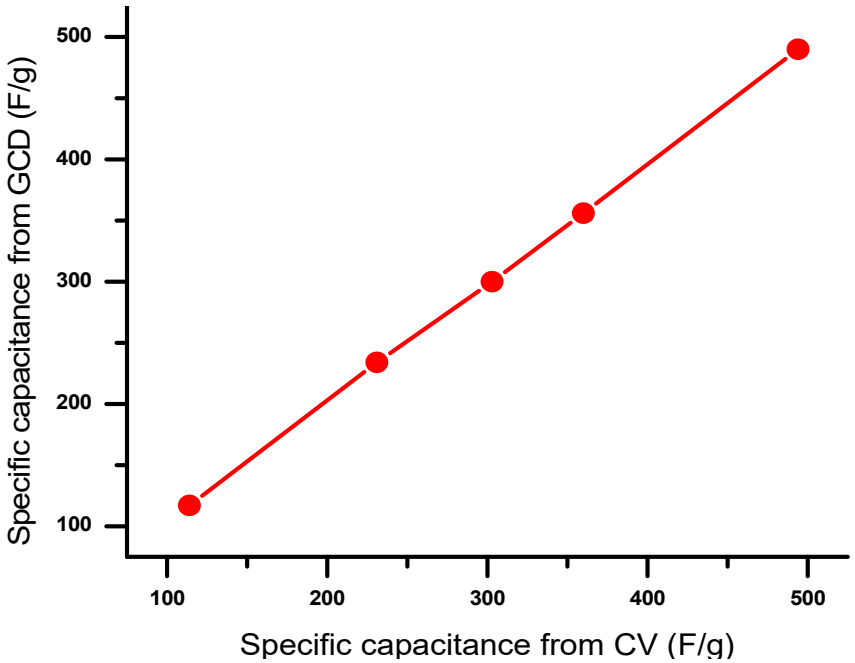

Figure 6: Correlation between C_{sp} values obtained from CV and GCD at an Au electrode in 0.1 M TEAP/CH_2Cl_2.

To benchmark pseudocapacitive performance of BPy–DDQ CT complex, its C_{sp} was compared with representative materials reported in recent literature [19-22].

Transition metal oxides and hybrid composites can exhibit very high capacitance values, sometimes exceeding 1000 F/g under optimized conditions, due to rich faradaic redox activity [19]. Redox-active materials such as NiO, V_2O_5 and MXenes typically show capacitance values in the range from 200 to 800 F/g depending on composition and testing conditions [20, 21]. Covalent organic frameworks and related organic systems generally display capacitance values ranging from ~100 to 800 F/g, with higher values reported for optimized conductive architectures [22]. BPy-DDQ CT complex delivers C_{sp} values from 494 to 114 F/g (CV) and 490 to 117 F/g (GCD) over scan rates from 0.025 to 0.40 V s^{-1}, placing it within the typical range of many pseudocapacitive materials, and supporting its promising charge-storage capability.

Coulombic efficiency

Coulombic efficiency (η) of CT complex was evaluated from GCD profiles according to the ratio of discharge to charge time. Calculated η values were consistently close to 100%, indicating highly reversible redox processes and minimal energy loss during cycling [14, 38]. This near-ideal efficiency confirms that pseudocapacitive behavior of CT complex arises from rapid and reversible faradaic reactions rather than from parasitic side reactions. Excellent coulombic efficiency further demonstrates the structural stability and robust electron-transfer kinetics of CT complex under repeated charge-discharge cycles [46-50]. From obtained results, combined electrochemical analysis demonstrates the potential of CT complex as an efficient and tunable material for application in supercapacitors and related energy storage devices, as presented in Fig. 7.

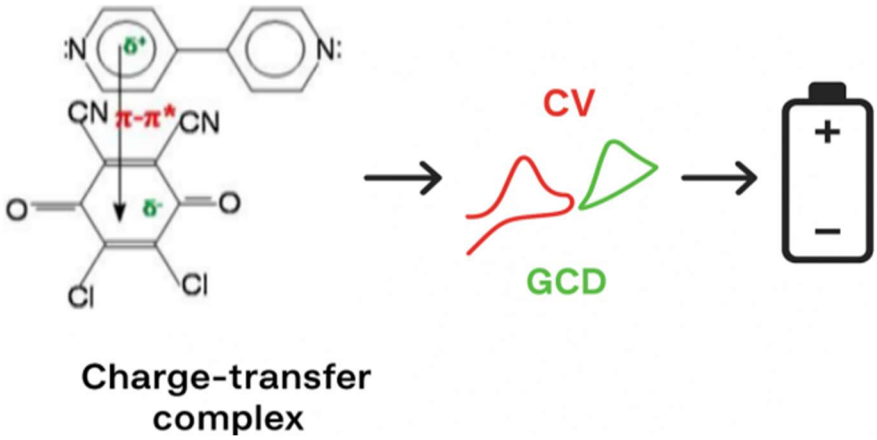

Figure 7: Schematic illustration of CT complex as an active electrode material for energy storage.

Tafel analysis and kinetic parameter determination

Resulting polarization curves, recorded in a conventional three-electrode configuration, were converted into Tafel plots to determine kinetic parameters of

electrode reactions [51, 52]. Potentials were first corrected to reversible hydrogen electrode (RHE) scale, and overpotential (η) was obtained according to Eq. (7):

$$\eta = E_{\text{measured}} - E_{\text{eq}} \quad (7)$$

where E_{eq} is thermodynamic equilibrium potential for the reaction of interest, calculated via Nernst equation. For hydrogen evolution reaction (HER) in acidic media, E_{eq} was taken as 0.000 V *vs*. RHE [53]. The relationship between overpotential (η) and logarithmic current density (j) is described in Eq. (8):

$$\eta = a + b \log(j) \quad (8)$$

where a is intercept and b Tafel slope. Linear region of the plot was identified in kinetic control regime, avoiding low-overpotential regions dominated by capacitive currents and high-overpotential regions influenced by mass transport limitations. Linear regression was applied within the refined range to obtain the slope (b) and intercept (a) (Fig. 8).

Exchange current density (j_0) was determined by extrapolating Tafel line to $\eta = 0$, according to Eq. (9) [54]:

$$j_0 = 10^{-a/b} \quad (9)$$

Higher j_0 values indicate greater intrinsic catalytic activity. Charge transfer coefficient (α) was calculated using Eq. (10):

$$b = \frac{2.303\,RT}{\alpha n F} \quad (10)$$

where n is the number of electrons transferred, R is gas constant, T is temperature, and F is Faraday constant. For HER at 298 K, this is simplified to Eq. (11):

$$b(\text{V/dec}) \approx \frac{0.0591}{\alpha n} \quad (11)$$

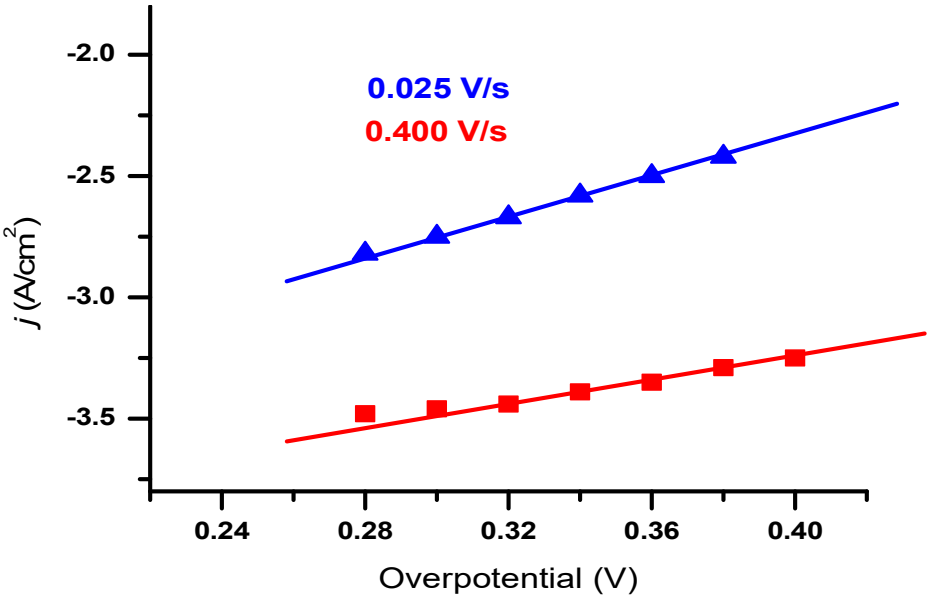

Figure 8: Logarithmic current density (log j) versus overpotential (η/V) at an Au electrode in 0.1 M TEAP/CH_2Cl_2, recorded at scan rates of 0.025 and 0.4 V/s.

The combination of Tafel slope, exchange current density and charge transfer coefficient provides a comprehensive kinetic description of the electrode process, enabling both mechanistic interpretation and quantitative comparison of catalytic performance.

From analyzed Tafel plot, linear fitting of optimal anodic region yielded a Tafel slope of 164 and 208 mV/dec for both scan rates of 0.025 and 0.400 V/s, respectively, which is characteristic of a quasireversible electron-transfer process [55]. Using standard Tafel relationship, this slope corresponds to a charge-transfer coefficient (α) of approxim. 0.361 and 0.283 for 0.025 and 0.400 V/s, respectively, at 298 K, assuming a one-electron transfer step. Extrapolation of linear fit to equilibrium potential provided an exchange current density (j_o) of 8.49×10^{-3} and 2.7×10^{-4} A/cm² at scan rates of 0.025 and 0.400 V/s, respectively. Obtained value of exchange current density (j_0) reflects intrinsic catalytic activity of the electrode toward the studied electrochemical reaction, since it represents the rate of electron transfer at equilibrium without any external driving force. Measured value of exchange current density at the scan rate of 0.025 V/s means that a large number of active sites are readily available for charge transfer, and that the reaction proceeds with minimal kinetic barriers. This indicates that the electrode material possesses excellent intrinsic catalytic activity, facilitating fast adsorption-desorption and electron transfer steps, which are essential for enhancing overall reaction kinetics. In contrast, at a higher scan rate of 0.400 V/s, j_o decreased significantly to 2.7×10^{-4} A/cm². The marked reduction suggests that catalyst activity is scan-rate dependent, where faster potential sweeps impose kinetic and mass transport limitations, restricting full engagement of surface-active sites. Thus, obtained j_0 confirms favorable electrocatalytic properties of the studied system [56, 57]. Furthermore, exchange current density (j_0) obtained from Tafel analysis was found to be in close agreement with values of 7.4×10^{-3} and 2.3×10^{-4} A/cm² calculated using Eq. (12):

$$j_0 = nFk^0C \quad (12)$$

The small difference between the two values can be attributed to experimental uncertainties, electrode surface heterogeneity, or deviations from ideal kinetic assumptions in Tafel model. Nevertheless, close correspondence indicates that the electrochemical process is well-described by the proposed kinetic framework, and the electrode exhibits reliable and consistent behavior across both experimental and theoretical approaches. Typical exchange current densities for non-precious HER catalysts are reported in the range from 10^{-5} to 10^{-3} A/cm², while state-of-the-art Pt-based catalysts reach ~10^{-2} A/cm² [58]. The obtained j_0 of 8.49×10^{-3} A/cm² at low scan rate therefore approaches the activity of noble-metal catalysts, highlighting excellent intrinsic kinetics of the studied system. Although the value decreases at higher scan rates, it remains above the level commonly reported for many transition-metal catalysts [59], suggesting that the material maintains a competitive activity profile. Thus, results confirm that

investigated CT complex possesses intrinsically high activity, though its effectiveness is partially constrained by kinetic and transport effects under rapid dynamic conditions.

In this study, it was observed that, for quasi-reversible electrochemical systems, parameters obtained from CV are significantly affected by the applied scan rate. As the scan rate increases, peak potential separation (ΔE_p) typically widens due to finite electron-transfer kinetics, reflecting a reduction in heterogeneous rate constant (k^0). Since exchange current density is directly proportional to heterogeneous rate constant, according to Eq. (12), a decrease in k^0 leads to a corresponding decrease in , value of j_0. This behavior was clearly observed in the measurements, where j_0 decreased from 8.49×10^{-3} A/cm^{2,} at a low scan rate (0.025 V/s), to 2.7×10^{-4} A/cm^2, at a higher scan rate (0.40 V/s).

Conclusion

Electrochemical investigation of CT complex presented in this study underscores its strong potential as an efficient and tunable material for next-generation energy storage devices. The unique redox properties of CT complex, combined with its favorable charge-storage behavior and rapid kinetics, were confirmed through CV, GCD conversion and Tafel analysis, which together provided clear insights into electron transfer efficiency and exchange current density. Proposed methodological framework linking CV-derived GCD profiles with Tafel plots offers a robust approach for correlating pseudocapacitive performance with charge-transfer kinetics, thereby enabling more accurate evaluation of their specific capacitance from a single dataset. These findings not only validate the versatility of CT complex for supercapacitors and electrocatalytic applications, but also highlight its promise as low-cost, sustainable alternative to conventional electrode materials in advanced energy storage and conversion systems.

Authors' contributions

I. S. El-Hallag: suggested the idea of the article; performed the experimental part. **A. A. Al-Owais**: wrote the article; elucidated obtained results. **S. H. El-Mossalamy**: revised the article; provided the compound under consideration.

Statements and declarations

The authors declare that they have no known competing financial interests or personal relationships that could have appeared to influence the work reported in this paper.

Funding

Not applicable.

Conflict of interests

The authors declare no conflict of interest.

Abbreviations

AgCl: silver chloride
BPy: 4,4′-bipyridine
C_{sp}: Gravimetric specific capacitance
CT: Charge transfer
CV: cyclic voltammetry
DDQ: 2,3-Dichloro-5,6-dicyano-1,4-benzoquinone
DL: Double-layer
E_{eq}: Equilibrium potential
ESD: Energy storage devices
GCD: Galvanostatic charge-discharge
HER: Hydrogen evolution reaction
i_p: peak current
j_0: Exchange current density
k^0: heterogeneous electron transfer rate
QR: Quasi-reversible
S: surface electrode area
SR: scan rate
TEAP: Tetraethylammonium perchlorate

Symbols definitions

α: charge-transfer coefficient
η: Coulombic efficiency

References

1. Mulliken RS. Molecular compounds and their spectra. II. J Am Chem Soc. 1952;74(3):811-24. https://doi.org/10.1021/ja01123a067
2. Yam WW, Chan AK-W, Hong EYH. Charge-transfer processes in metal complexes enable luminescence and memory functions. Nat Rev Chem. 2020;4(10):325-40. https://doi.org/10.1038/s41570-020-0199-7
3. Jurchescu OD, Goetz KP, Vermeulen D et al. Charge-transfer complexes: new perspectives on an old class of compounds. J Mater Chem C. 2014;2(22): 5372-83. https://doi.org/10.1039/C3TC3206
4. Goetz KP, Vermeulen D, Payne ME et al. Charge-transfer complexes: new perspectives on an old class of compounds. J Mater Chem C. 2014;2(13):3065-76. https://doi.org/101039/C3TC32062F
5. Kaim W, Fiedler J. Spectroelectrochemistry: the best of two worlds. Chem Soc Rev. 2009;38(12):3373-82. https://doi.org/10.1039/B821778J
6. Shukla R, Ghosh HN. Charge transfer complexes and their photophysics. Chem Rev. 2017;117(21):8404-39. https://doi.org/10.1021/acs.chemrev.6b00536

7. Nicholson RS. Theory and application of cyclic voltammetry for measurement of electrode reaction kinetics. Analyt Chem. 1965;37(10):1351-55. https://doi.org/10.1021/ac60230a016
8. Heinze J. Cyclic voltammetry Electrochemical spectroscopy Angew Chem Int Ed. 1984;23(9):831-47. https://doi.org/10.1002/anie.198408311
9. Bard AJ, Faulkner LR. Electrochemical Methods: Fundamentals and Applications, Wiley, New York, 2001.
10. Gosser DK. Cyclic Voltammetry: Simulation and Analysis of Reaction Mechanisms, VCH, New York, 1993;1-293.
11. Wang J. Analytical Electrochemistry, Wiley-VCH, Hoboken, 2006;1-216.
12. Bard AJ, Stratmann M, (Eds.) Encyclopedia of Electrochemistry, Vol. 1: Instrumentation and Electroanalytical Chemistry, Wiley-VCH, Weinheim, 2002; 1-800.
13. Conway BE. Electrochemical Supercapacitors: Scientific Fundamentals and Technological Applications, Springer, New York, 1999; 1-698
14. Simon P, Gogotsi Y. Materials for electrochemical capacitors. Nat Mater. 2008;7(11):845-54. https://doi.org/10.1038/nmat2297
15. Stoller MD, Ruoff RS. Best practice methods for determining an electrode material's performance for ultracapacitors. Ener Environ Sci. 2010;3(9):1294-1301. https://doi.org/10.1039/C0EE00074D
16. El-Kady MF, Kaner RB. Scalable fabrication of high-power graphene micro-supercapacitors for flexible and on-chip energy storage. Nat. Commun. 2013;4(1-8):1475. https://doi.org/10.1038/ncomms2446
17. Wang Y, Song Y, Xia Y. Electrochemical capacitors: mechanism, materials, systems, characterization and applications. Chem Soc Rev. 2016;45(22):5925-50. https://doi.org/10.1039/C5CS00580A
18. Augustyn V, Simon P, Dunn B. Pseudocapacitive oxide materials for high-rate electrochemical energy storage. Energy Environ Sci. 2014;7(4):1597-1614. https://doi.org/10.1039/C3EE44164D
19. Ahmad AM. Cyclic voltammetry of hybrid supercapacitors: A characterization review. Inorg Chem Commun. 2025;172:113677. https://doi.org/10.1016/j. inoche. 2024.113677
20. Yi-Min W, Kulurumotlakatla D K, Long Z et al. Pseudocapacitive materials for energy storage: properties, mechanisms, and applications in supercapacitors and batteries. Front Chem. 2025;13:1636683. https://doi.org/10.3389/fchem.2025.1636683
21. Sanju G, Sara B. C, Bryce A. Designing high-performance asymmetric and hybrid energy devices via merging supercapacitive/pseudopcapacitive and Li-ion battery type electrodes. Sci Rep. 2024;14:29277. https://doi.org/10.1038/ s41598-024-79622-6
22. Shen X, Jinghang W, Xiang W et al. Recent advances in the utilization of covalent organic frameworks (COFs) as electrode materials for supercapacitors. Chem. Sci. 2023,14:13601. https://doi.org/10.1039/d3sc04571d

23. Yang S, Guo Y, Liu T et al. Supramolecular charge-transfer complexes for electrochemical energy storage. Chem Soc Rev. 2021;50(24):9391-9423. https://doi.org/10.1039/D1CS00217K
24. Yamada H, Makuta Y, Kumai R et al. Supramolecular charge-transfer complexes with tunable electrochemical properties. Chem Eur. J. 2020;26(18):5203-11. https://doi.org/10.1002/chem.202000306
25. Wang Y, Song Y, Xia Y. Electrochemical capacitors: mechanism, materials, systems, characterization and applications. Chem Soc Rev. 2016;45(22):5925-50. https://doi.org/10.1039/C5CS00580A
26. Briegleb G. Electronen-Donator-Acceptor-Komplexe, Springer-Verlag, Berlin, 1961. https://doi.org/10.1007/978-3-642-45866-8
27. Foster R. Organic Charge-Transfer Complexes, Academic Press, London, 1969. https://doi.org/10.1016/C2013-0-02777-3
28. Rosokha SV, Kochi JK. Fresh look at electron transfer mechanisms via the donor/acceptor bindings in precursor complexes. Acc Chem Res. 2008;41(5):641-653. https://doi.org/10.1021/ar700263h
29. Bryce MR. Recent progress on conducting organic charge-transfer salts, Chem Soc Rev. 1991;20(3):355-390. https://doi.org/10.1039/CS991200035526
30. Ferraris J, Cowan DO, Walatka V et al. Electron transfer in a new highly conducting donor–acceptor complex. J Am Chem Soc. 1973;95(3):948-49. https://doi.org/10.1021/ja00783a082
31. Hush NS. Intervalence-transfer absorption. Part 2. Theoretical considerations and spectroscopic data. Prog Inorg Chem.1967;8:391-444. https://doi.org/10.1002/9780470166077.ch7
32. Kato R. Conducting metal–organic frameworks and charge-transfer salts. Chem Rev. 2004;104(11):5319-46. https://doi.org/10.1021/cr0306428
33. Nishijo J, Okabayashi T. Electrochemical aspects of charge-transfer complexes. Bull Chem Soc Jap. 1981;54(5):1389-93. https://doi.org/10.1246/bcsj.54.1389
34. Kochi JK. Charge transfer and transport in donor/acceptor molecular systems. Adv Phys Org Chem. 2000;35:193-318. https://doi.org/10.1016/S0065-3160(00)35005-5
35. Yamada J, Sugimoto T. Charge Transfer Salts: Structural Aspects and Properties, Springer-Verlag, Berlin, 1998. https://doi.org/10.1007/978-3-642-72069-3
36. Mas-Torrent M, Rovira C. Role of molecular order and solid-state structure in organic field-effect transistors. Chem Rev. 2011;111(8):4833-56. https://doi.org/10.1021/cr100436j
37. Shida T, Hamill WH. Charge-transfer states and exciplexes in solution. J Chem Phys. 1966;44(5):1736-43. https://doi.org/10.1063/1.1726920
38. Miller JR, Simon P. Electrochemical capacitors for energy management. Science. 2008;321(5889):651-52. https://doi.org/10.1126/science.1158736

39. Salunkhe RR, Kaneti YV, Yamauchi Y. Metal–organic framework-derived nanoporous metal oxides toward supercapacitor applications: Progress and prospects. ACS Nano. 2017;11(6):5293-5308. https://doi.org/10.1021/acsnano.7b02796
40. Béguin F, Presser V, Balducci A et al. Carbons and electrolytes for advanced supercapacitors. Adv Mater. 2014;26(14):2219-51. https://doi.org/10.1002/adma.201304137
41. Zhai Y, Dou Y, Zhao D et al. Carbon materials for chemical capacitive energy storage. Adv Mater. 2011;23(42):4828-50. https://doi.org/10.1002/adma.201100984
42. Toupin M, Brousse T, Bélanger D. Charge storage mechanism of MnO_2 electrode used in aqueous electrochemical capacitor. Chem Mater. 2004;16(16):3184-90. https://doi.org/10.1021/cm049649j
40. Brousse T, Bélanger D, Long JW. To be or not to be pseudocapacitive. J Electrochem Soc. 2015;162(5):A5185-89. https://doi.org/10.1149/2.0201505jes
44. Wang H, Casalongue HS, Liang Y et al. $Ni(OH)_2$ nanoplates grown on graphene as advanced electrochemical pseudocapacitor materials. J Electrochem Soc. 2010;132(21):7472-77. https://doi.org/10.1021/ja102267j
45. Chodankar NR, Kaneti YV, Nanjundan AK et al. Rational design of hierarchical porous carbons for supercapacitors and capacitive energy storage. Chem Soc Rev. 2022;51(4):2337-82. https://doi.org/10.1039/D1CS00776F
46. Dubal DP, Ayyad O, Ruiz V et al. Hybrid energy storage: The merging of battery and supercapacitor chemistries. Chem Soc Rev. 2015;44(3):1777-90. https://doi.org/10.1039/C4CS00266K
47. Zhang F, Zhang T, Yang X et al. Recent advances in supercapacitor electrode materials. Nanoscale. 2013;5(15):6930-39. https://doi.org/10.1039/C3NR00040K
48. Yu Z, Tetard L, Zhai L et al. Supercapacitor electrode materials: Nanostructures from 0 to 3 dimensions. Ener Environ Sci. 2015;8(3):702-30. https://doi.org/10.1039/C4EE03229B
49. Choudhury A, Goswami A, Dutta S et al. Insights into charge storage in pseudocapacitors. J Mater Chem A. 2021;9(44):22895-930. https://doi.org/10.1039/D1TA06106E
50. Zhang LL, Zhao XS. Carbon-based materials as supercapacitor electrodes. Chem Soc Rev. 2009;38(11):2520-31. https://doi.org/10.1039/B813846J
51. Zheng Y, Jiao Y, Jaroniec M, et al. Advancing the electrochemistry of the hydrogen-evolution reaction through combining experiment and theory. Angew Chem Intern Edit. 2015;54(1):52-65. https://doi.org/10.1002/anie.201409740

52. Tafel J. Über die Polarisation bei kathodischer Wasserstoffentwicklung. Zeitschr Phys Chem. 1905;50(1):641-712. https://doi.org/10.1515/zpch-1905-5033
53. Sheng W, Gasteiger HA, Shao-Horn Y. Hydrogen oxidation and evolution reaction kinetics on platinum: acid vs alkaline electrolytes. J Electrochem Soc. 2010;157 (11):B1529-36. https://doi.org/10.1149/1.3483106
54. Conway BE, Bai L. Determination of kinetic parameters of HER at high overvoltages. J Electroanalyt Chem. 1983;146(1-2):189-202. https://doi.org/10.1016/S0022-0728(83)80579-0
55. Zheng J, Yan Y, Xu B. Correcting the hydrogen diffusion limitation in rotating disk electrode measurements of hydrogen evolution reaction kinetics, J Electrochem Soc. 2015;162(14):F1470-81. https://doi.org/10.1149/2.0191514jes
56. Parsons R, Hale P. The kinetics of hydrogen evolution at platinum in acid solutions. J Electroanalyt Chem. 1972;39(2):163-77. https://doi.org/10.1016/S0022-0728(72)80486-8
57. Trasatti S, Petrii OA. Real surface area measurements in electrochemistry. Pure Appl Chem. 1991;63(5):711-34. https://doi.org/10.1351/pac199163050711
58. Trasatti S. Electrocatalysis in the anodic evolution of oxygen and chlorine, Electrochim Acta. 1984;29(11):1503-12. https://dx.doi.org/10.1016/0013-4686(84)85004-5
59. Conway BE, Tilak BV. Interfacial processes involving electrocatalytic evolution and oxidation of H_2, and the role of chemisorbed H. Electrochim Acta. 2002;47(22-23):3571-94. https://dx.doi.org/10.1016/S0013-4686(02)00329-8